Mathematical Biology and Bioinformatics
2015. V. 10. № 2. P. 372–386. doi: 10.17537/2015.10.372

========== MATHEMATICAL MODELING ==========

UDK: 530.1: 537.226.4+541.1+577

Analysis of the computational and experimental studies of the polarization switching in the PVDF and P(VDF-TrFE) ferroelectric films at the nanoscale

Bystrov V.S.[*1], Paramonova E.V.[1], Bystrova A.V.[1], Gevorkyan V.E.[2], Meng X.J.[3], Tian B.B.[3], Wang J.L.[3], Avakyan L.A.[2]

[1]*Institute of Mathematical Problems of Biology RAS, Pushchino, Moscow Region, Russia*
[2]*Southern Federal University, Physical Faculty, Rostov-on-Don, Russia*
[3]*Shanghai Institute of Technical Physics, Chinese Academy of Sciences, Shanghai, China*

Abstract. In this paper, molecular models are used to investigate and analyze the polarization switching in the polyvinylidene fluoride (PVDF) and poly(vinylidene fluoride-trifluoroethylene) (P(VDF-TrFE)) Langmuir-Blodgett (LB) nanofilms, in comparison with the experimental data at the nanoscale. Quantum-mechanical calculations and modeling, as well as molecular dynamics (MD) simulations based on semi-empirical quantum-chemical methods (such as PM3), show that the energy of the studied PVDF and P (VDF-TrFE) molecular structures, and their polarization switching proceed by the intrinsic homogeneous switching mechanism in the framework of the phenomenological theory of Landau-Ginzburg-Devonshire (LGD) in the linear approximation at low values of the electric field. The magnitude of the resulting critical coercive field is within the E_C ~ 0.5 ... 2.5 GV/m, which is consistent with experimental data. It is also found that the uniform polarization switching mechanism of the polymer chains PVDF and P (VDF-TrFE) is due to the quantum properties of the molecular orbitals of the electron subsystem. This is clearly seen in both the polarization hysteresis loops, and the total energy changes. In this case, the turnover chain time, obtained by molecular dynamics within semi-empirical quantum-chemical PM3 approach in a limited Hartree-Fock approximation, when approaching this critical point, increases sharply, tending to infinity, which corresponds to the theory of LGD. Otherwise, at the high values of the applied electric field the polarization switching correspond to the extrinsic domain mechanism in the frame of the microscopic Kolmogorov–Avrami–Ishibashi (KAI) theory, describing bulk ferroelectric crystals and thick films. The performed analysis of computational and experimental data allows us to estimate the critical sizes of the possible transition region approximately on the order of 10 nm between intrinsic homogeneous and extrinsic domain switching mechanisms.

Key words**:** *polymer ferroelectric, polarization switching, computer simulation, molecular dynamics, quantum-mechanical calculations.*

[*]vsbys@mail.ru

1. INTRODUCTION

Polymer ferroelectric thin Langmuir-Blodgett (LB) films, based on poly(vinylidene fluoride) (PVDF) and poly(vinylidene fluoride-trifluoroethylene) P(VDF-TrFE) copolymers, clearly demonstrated polarization switching phenomena on nanometer size scale with local ferroelectric polarization reversal on the atomic-molecular level [1–5]. Now these LB polymer films are widely explored experimentally, using various techniques, including nanoscale characterization by atomic force microscopy (AFM) and piezoresponse force microscopy (PFM) method [4–11], and theoretically, using various computational methods [12–21]. These novel ferroelectric nano-materials are very promising for nanobiotechnology, nanobiomedicine, bio- and microelectronics, and as a prospective component of various nano-composites and "intellectual" templates with "smart surface" properties. Having high compatibility with many organic and biological molecules and tissues they possess appropriate acoustic and piezoelectric properties [22–24]. One promising idea is to use actuators made from biocompatible polyvinylidene fluoride (PVDF) piezoelectric materials [25] since they demonstrate high surface charge – polarization of PVDF / P(VDF-TrFE) and its switching under specific external influences, such as changes of an external electric field. Nevertheless many of these important physical and structural properties of the PVDF copolymers thin films are not clear yet, especially the dependence of their polarization switching properties on the size or width of these polymer films. One of the main questions now is how to determine the critical size for the transition (crossing, going over) between homogeneous and domain switching mechanisms [4, 5, 11, 20], or transition of the polarization switching from the extrinsic to intrinsic mechanisms in these ultrathin polyvinylidene fluoride homopolymer films.

In this paper we report our studies of polarization switching properties of PVDF copolymer films with the use of molecular modeling from first principles and measurements of experimental AFM/PFM and plane capacitances of the polymer films [8–11]. These studies continue the series of our previous investigations of ferroelectric and nanoscale properties of thin LB PVDF copolymer films [8, 16–21]. The analysis of computational and experimental data and new computed evaluations obtained allow us to estimate the sizes of possible transition region approximately to be of the order of 10 nm.

The new data obtained can be used in various fields of nanobioelectronics and bionanomedicine, particularly in the development of new actuators and templates, such as built-in sensors and new smart surfaces for medicine, environmental and ecology control, etc.

2. INTRINSIC HOMOGENEOUS POLARIZATION SWITCHING

As is known the discovery of LB ferroelectric films [1–5] made it possible to change the thickness of LB ferroelectric polymeric PVDF films with accuracy of an elementary unit cell or one monolayer (0.5 nm) and to indicate its polarization switching with thickness of two monolayers (1 nm) [2, 5]. The existence of switching in such LB ferroelectric polymers at the nanoscale with thickness of the same order of magnitude as the critical domain nucleus [26] led in turn to the development of the phenomenological Landau-Ginzburg-Devonshire (LGD) theory of ferroelectricity as concerns the homogeneous switching mechanism [27]. This approach shows that intrinsic homogeneous polarization switching of the polymeric ferroelectric films at the nanoscale has a critical character and reveals a critical point at the LGD coercive field $E = E_C$ [27]:

$$\tau^{-2} = C \cdot \left(E - E_C \right), \tag{1}$$

where τ is switching time, E is the external electric field, and E_C is the LGD coercive field, and C is constant [27].

Thus LGD phenomenological switching, developed in [27], shows that in low electric field's limit the magnitude τ^{-2} demonstrates a linear behavior with the rise of E. This result differs drastically from a known microscopic domain Kolmogorov-Avrami-Ishibashi (KAI) mechanism [28–30], which is valid for more bulk ferroelectric crystals and thick films. The LGD intrinsic coercive field E_C was found experimentally in copolymer thin films at the nanoscale [31]. Further experiments indicated that bulk polymeric ferroelectric films behave in accordance with KAI switching mechanism, while the nanoscale films reveal homogeneous LGD switching [12, 13, 27].

Computational studies of the polarization switching mechanism in such polymer films were performed on an idealized model, consisting of one, two and four polymer chains with limited structural units by means of the first-principles quantum theory [15–21].

Now we try to analyze all these approaches using both experimental data and computed values, and try to improve further some of the methods to reach a more adequate consensus on the value of the critical size or width for transition between intrinsic homogeneous and extrinsic domain switching mechanisms, correponding to the relation between LGD and KAI theoretical views.

3. ELECTRIC FIELD DISTRIBUTION INSIDE FERROELECTRIC SAMPLES

First, we will perform an analysis of the main experimental situations that occur during measurements of polarization in the ferroelectric samples. Usual experimental setup for investigation of how polarization depends on an applied electrical field consists of two parallel metallic electrodes between which ferroelectrics (or dielectrics) are introduced – it is a usual plane capacitor with two parallel plane electrodes. In this case, inside such capacitor the electric field is homogenous and uniform with parallel electrostatic isolines in the main volume. Only at small distances on the sides of the capacitor the uniformity can be disturbed. Another situation arises under AFM/PFM tip inside the samples. The main difference is caused by very high non-uniformity and non-homogeneity of the electric field under narrow AFM/PFM tip inside the sample. Now we consider and analyze these two main experimental situations in greater detail.

3.1. Electric field distribution under AFM/PFM tip inside a ferroelectric sample

Let us consider a scheme of the electric field inside the sample, showed in Fig. 1. Such scheme is usually used for the description of an electric field distribution inside any samples under AFM/PFM tip, since the electric field has a very non-uniform and un-homogeneous distribution, but it can be approximated by semi-ellipsoidal form of polarization in that arises in some region called a polar domain. A similar distribution can describe the domain with the polarization switching between the ferroelectric (with polarization P) and surrounded the paraelectric ($P = 0$) phases, or switching of the orientation in ferroelectric phase from P to the oppositely oriented polarization equal to minus P. The mathematical formulae for these descriptions were proposed in papers [32, 33].

From these papers we can see that the **electric field under the tip is un-homogeneous** [32, 33]:

$$E(r) = \frac{1}{2\pi\varepsilon_0}\left(\frac{C_t U}{\sqrt{\varepsilon_a \varepsilon_c}+1}\right)\sqrt{\frac{\varepsilon_a}{\varepsilon_c}}\,\frac{(R+\delta)}{\left[(R+\delta)^2 + r^2\right]^{3/2}},\ r^2 = z^2 + \rho^2, \qquad (2)$$

where R is the tip radius, δ is the distance from the tip to sample surface, U is applied voltage, and r, z, ρ are the coordinates in the cylindrical system.

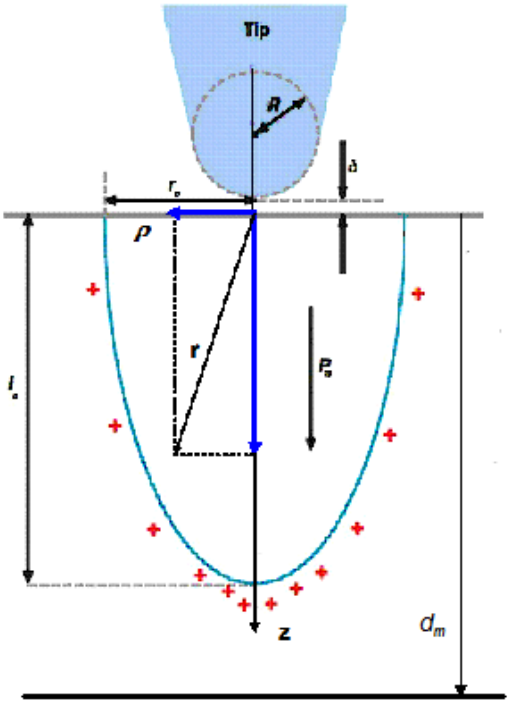

Fig. 1. Scheme of the domain under tip.

The traditional notation is:

$$k = \sqrt{\varepsilon_a \varepsilon_c}\ ,\ \gamma = \sqrt{\frac{\varepsilon_a}{\varepsilon_c}}\ , \tag{3}$$

ε_c and ε_a are the dielectric constants in directions parallel and perpendicular to the polar axis, respectively. Capacitance for such a configuration can be calculated using the formula from paper [34]:

$$C_t = 4\pi\varepsilon_0 R \frac{k+1}{k-1} \ln\left(\frac{k+1}{2}\right), \tag{4}$$

and total charge is $Q = C_t U$, where U is voltage on the AFM/PFM tip.

The normal component of the electric field in these coordinates is E_n ($\rho = 0$, $r = z$) [32–34]:

$$E_n = \frac{1}{2\pi\varepsilon_0}\left(\frac{C_t U}{k+1}\right)\gamma \frac{R+\delta+\gamma z}{\left[\left(R+\delta+\gamma z\right)^2\right]^{3/2}} = \frac{1}{2\pi\varepsilon_0}\left(\frac{C_t}{k+1}\right)\gamma U \frac{1}{\left(R+\delta+\gamma z\right)^2}. \tag{5}$$

Substitution of the C_t from (4) to (5) leads to the following relation:

$$E_n = \frac{2\ln\left(\frac{k+1}{2}\right)}{k-1}\gamma \frac{RU}{\left(R+\delta+\gamma z\right)^2}, \tag{6}$$

For usual simple approximation with $\delta = 0$ we obtain:

$$E_n = \frac{2\ln\left(\frac{k+1}{2}\right)}{k-1}\gamma \frac{RU}{\left(R+\gamma z\right)^2}. \tag{7}$$

For most simple cases with $\varepsilon_a = \varepsilon_c = \varepsilon$, $k = \varepsilon$, $\gamma = 1$ we can rewrite (7) as follows:

$$E_n = \frac{2\ln\left(\frac{\varepsilon+1}{2}\right)}{\varepsilon-1}\frac{RU}{\left(R+z\right)^2}. \quad (8)$$

Another most simplified approximation was made in paper [35] (Tybel and Triscone, see formulae (8) in the text at page 2 in that paper). They proposed the following simplified formula for the films with maximal thickness d_m, where dielectric permittivity is not taken into account:

$$E = \frac{UR}{zd_m}, \quad (9)$$

where z is the coordinate of the depth inside the film.

Below we present the results of calculations for the electric field distributions inside the samples using different approximations and cases.

The first 3 curves presented in Fig. 2 correspond to formula (8) with various $\varepsilon = 12$, 6, 1 and with the tip radius R = 10 nm, voltage U = 30 V. The forth curve in Fig. 2 corresponds to the Triscone formula (9) for maximal value d_m = 100 nm and without regard for ε. The last curve in Fig. 2 corresponds to equation (2) and (5) with $\varepsilon_a = 4$, $\varepsilon_b = 10$, and with $\delta = 0$ (which corresponds to the data from paper [32]). These figures (Fig. 2,*a* and 2,*b*) illustrate our computed data, which are especially close to the experimental values.

We know that the polarization switching to the opposite direction can be observed at the values of the intrinsic coercive field E_C = 1.0 … 2.5 GV/m [4–14, 16–21].

From our calculations it can be easily seen that these critical values are reached only for the cases when the depth is of the order of z = 10 nm, for the cases with $\varepsilon = 12$, which corresponds to formula (8). Another close curve corresponds to formulae (2) and (5) with values $\varepsilon_a = 4$, $\varepsilon_b = 10$, and with $\delta = 0$.

We must emphasize here that a similar critical size with distance $z_c = z$ = 10 nm, was directly experimentally observed in paper [11] (performed by the group of Prof. Meng), and was earlier estimated in paper [8] (by the group of Dr. Bystrov).

This critical size $z_c = z$ = 10 nm, is a very important parameter, at which the mechanism for the polarization switching changes from homogeneous mechanism described by the LGD theory to the extrinsic domain mechanism, which is described by KAI theory. The proposed transformation region with the sizes of the order of $z_c = z$ = 10 nm, must be investigated further in greater detail, because here some details of transferred region and molecular mechanism peculiarities are still to be clarified.

For example, here we can see that at the distances $z_c = z$ = 12 nm, the switching behavior can exist too, but for this case it takes place at a lower coercive field E_C = 1.0 … 2.0 GV/m (see on the Fig. 2,*b*).

Similar distributions are shown in the figures (Fig. 3) for the case with $\varepsilon = 9$, and for the different tip radii R and voltages U, computed using equation (7). The sizes at the distances $z_c = z$ = 10 nm are very close to the experimental values, but the sizes with distances $z_c = z$ = 12 nm and around it must be investigated further in greater detail too.

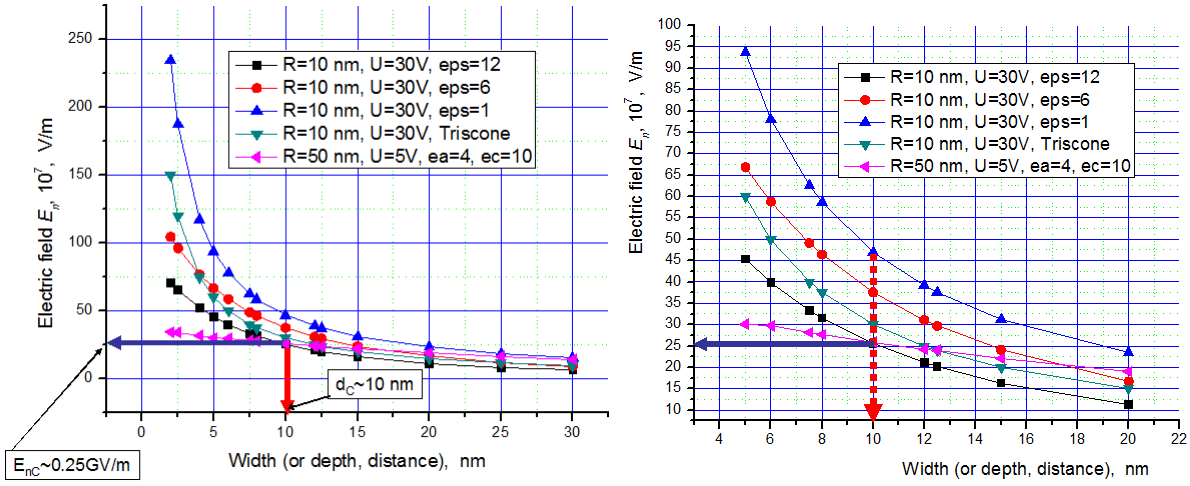

Fig. 2. Distributions of the normal component of electric field E_n inside a sample from depth z: ***a***) long depth, ***b***) short depth.

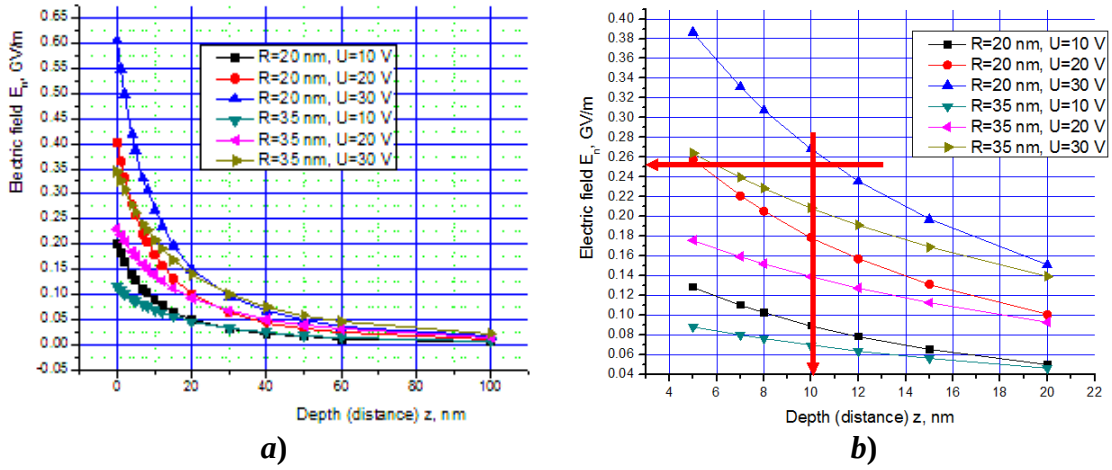

Fig. 3. Electric field E_n distribution in a sample under the tip from depth z using (7): ***a***) long depth, ***b***) short depth.

3.2. Electric field distribution inside the plane capacitor with a ferroelectric sample

Another case must be considered for the capacitor scheme which is usually used for experimental observation and measuring of the polarization dependence from the applied electric field (see for example in [11]). Such capacitor scheme is presented in Fig. 4.

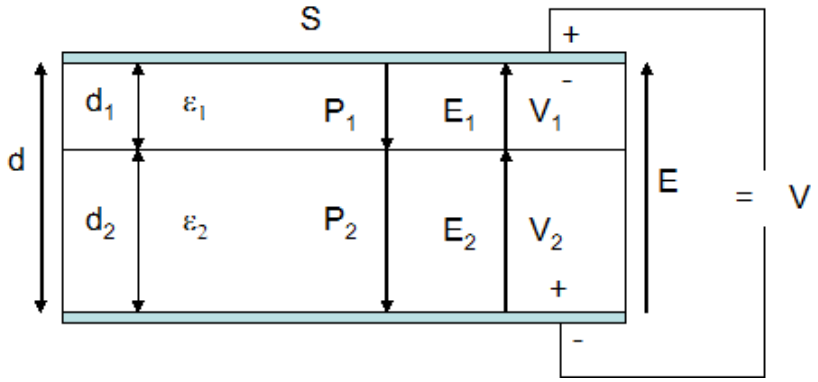

Fig. 4. Scheme of the capacitor measurements (here is the applied external field $E = E_0$, which is used in the equations below).

Usual reverse capacitance is described as follows (in the SI units):

$$\frac{1}{C_S} = \frac{d}{\varepsilon\varepsilon_0 S}, \tag{10}$$

$$\frac{1}{C_S} = \frac{V}{Q}, \tag{11}$$

where Q – charge, S – surface, V – voltage, $\varepsilon_0 = 8.854 * 10^{-12}$ F/m.

But since polarization is equal to $P = Q/S$, then, if we use $C = C_S/S$, and $C = P/V$, we obtain $\frac{1}{C} = \frac{d}{\varepsilon\varepsilon_0}$.

As a result, the equation of the total reverse capacitance is:

$$\frac{1}{C} = \frac{1}{C_1} + \frac{1}{C_2} = \frac{d_1}{\varepsilon_1\varepsilon_0} + \frac{d_2}{\varepsilon_2\varepsilon_0} = \frac{1}{\varepsilon_0}\left(\frac{d_1}{\varepsilon_1} + \frac{d_2}{\varepsilon_2}\right) = \frac{V}{P}. \tag{12}$$

On the other hand, for the induction D and the external field $E = E_0$ from boundary conditions we have $D = E_0 = \varepsilon_1 E_1 = \varepsilon_2 E_2 = P/\varepsilon_0$ and therefore:

$$V = V_1 + V_2 = E_1 d_1 + E_2 d_2 = \frac{D}{\varepsilon_1} d_1 + \frac{D}{\varepsilon_2} d_2 = \frac{P}{\varepsilon_0}\left(\frac{d_1}{\varepsilon_1} + \frac{d_2}{\varepsilon_2}\right). \tag{13}$$

Using $E_1 = \frac{\varepsilon_2}{\varepsilon_1} E_2$ we have

$$V = \frac{\varepsilon_2}{\varepsilon_1} E_2 d_1 + E_2 d_2 = E_2\left(d_1 \frac{\varepsilon_2}{\varepsilon_1} + d_2\right). \tag{14}$$

Therefore

$$E_2 = \frac{V}{d_2 + d_1 \frac{\varepsilon_2}{\varepsilon_1}}. \tag{15}$$

For $d_1 \to 0$, $E_2 \to \frac{V}{d_2}$, and because $E_0 = \varepsilon_2 E_2$, $\to$ $E_2 = \frac{E_0}{\varepsilon_2}$, and $E_0 = \varepsilon_2 \frac{V}{d_2} = \varepsilon_2 E_2$.

The main features are the following:

1. Electric field is homogeneous in all the space inside the capacitance volume, and therefore the polarization P inside any sample is homogeneous.

2. After connecting the capacitance with one layer (if $d_1 \to 0$) to voltage V, electric field inside is $E_2 \to \frac{V}{d_2}$. In this case the external field

$$E_0 = \varepsilon_2 \frac{V}{d_2} = \varepsilon_2 E_2. \tag{15a}$$

3. The value of the external electric field E_0 is larger than electric field E_2 inside the sample ($E_0 > E_2$).

If here is oxide layer $d_1 \neq 0$ with ε_1, the electric field inside a sample depends on its properties (as is shown in [4]) and is described again by equation (15):

$$E_2 = \frac{V}{d_2 + d_1 \dfrac{\varepsilon_2}{\varepsilon_1}} .$$

Using the data from work [11] for width of oxide layer d_1 = 1.6 nm, and for the PVDF with parameters $\varepsilon_2 \sim= 9$, $\varepsilon_1 \sim= 8$, we calculate now the dependence of the $E_2(d_2)$ (15) for various voltages V = 3, 5, 10 V. We performed similar calculations for some other values $\varepsilon_2 \sim= 10$, $\varepsilon_1 \sim= 5$. The results are presented in Fig. 5.

Fig. 5 shows that in both the cases critical parameters E_C, d_c depend on the voltage and reach their critical values at the smallest values of V.

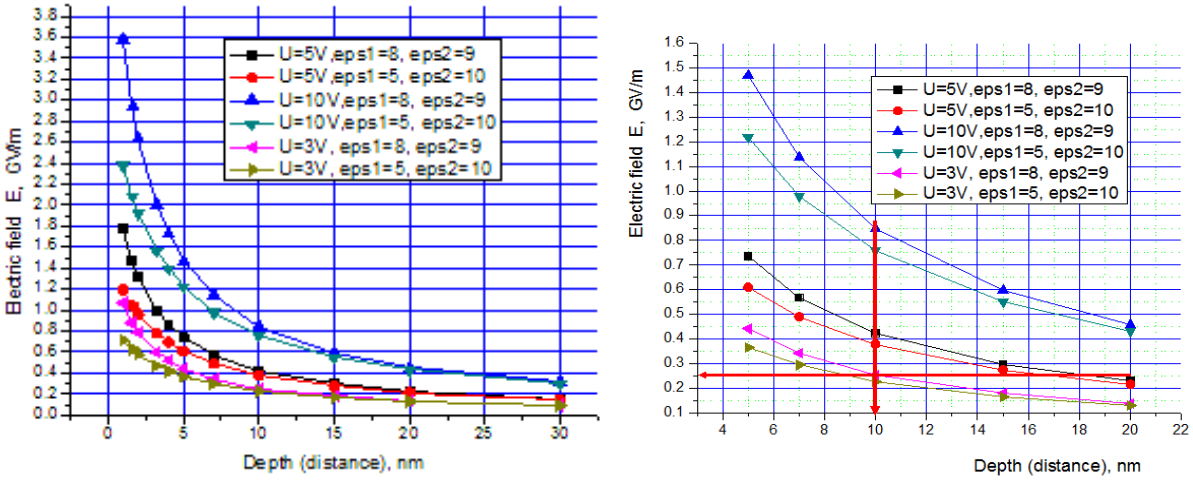

a) ***b***)

Fig. 5. Electric field dependence inside a plate capacitor sample from width for different dielectric permittivities and voltage according to formula (15): ***a***) long depth, ***b***) short depth.

4. MOLECULAR MODELING OF POLARIZATION SWITCHING IN PVDF

Molecular modeling of the PVDF and investigation of their polarization switching was performed in [20, 21]. In these cases of the computational molecular modeling using the HyperChem software we used a special option for imitation of the applied external electrical field [5]. It corresponds to some "simulation of effective electrodes", for example as is shown in Fig. 6.

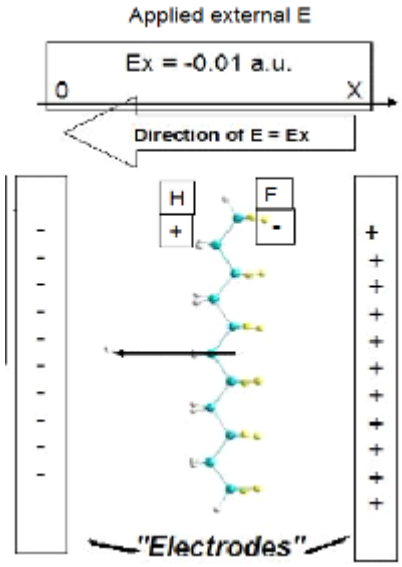

Fig. 6. Simulation of electrodes.

In another orientation of Cartesian axis the “work space” of HyperChem has the images from works [20, 21] (Fig.7).

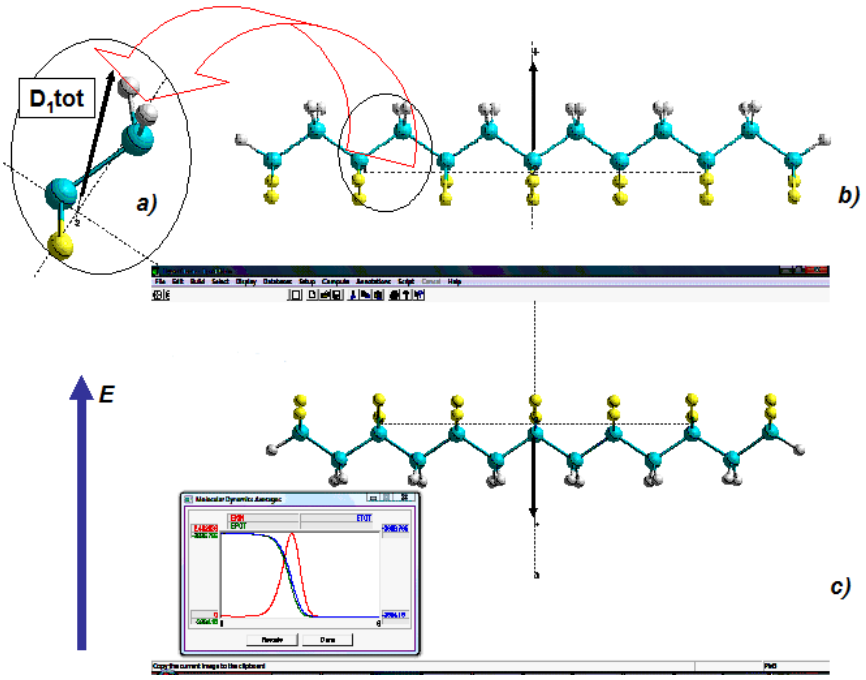

Fig. 7. Scheme of PVDF chain rotation in the applied external E field: ***a***) individual unit $C_2H_2F_2$ with unit dipole moment; ***b***) PVDF chain from 6 units; ***c***) PVDF chain was rotated in the opposite direction in the applied external electrical field E (image from the HyperChem “Work Space” in the case of the Molecular Dynamics (MD) simulation run with shown changes of energies in the insertion window.

In the framework of the Landau-Ginzburg-Devonshir (LGD) theory the switching time at the low electric field E could be represent in the linear approximation with critical $E = E_C$ [20, 27] as follows (see above the same equation (1))**:**

$$\tau^{-2} = C \cdot \left(E - E_C \right),$$

where C is a constant.

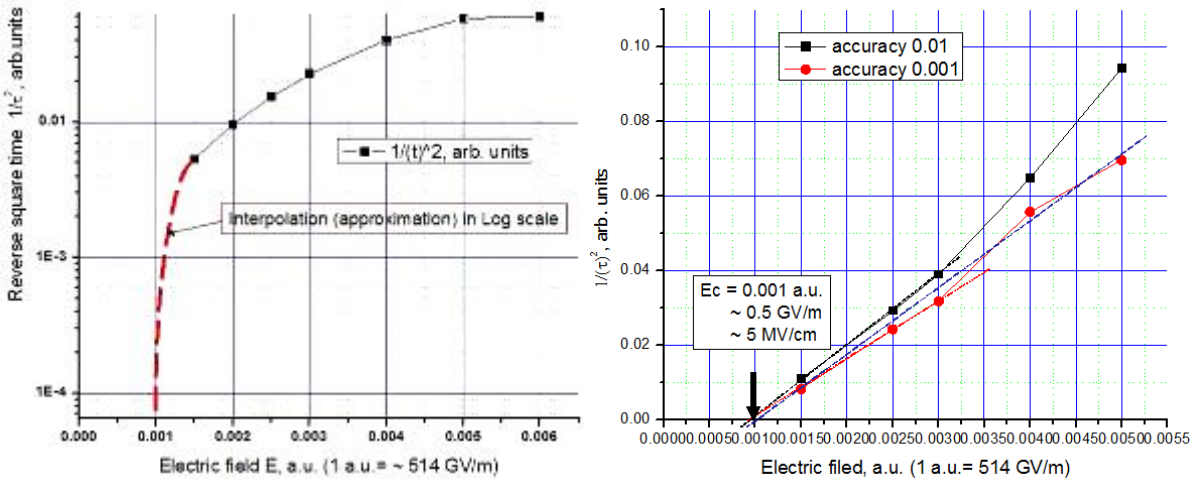

a) ***b***)

Fig. 8. Dependence of the reverse squared switching time from value of the applied electric field for 1 PVDF chain consisting of 6 elementary units: ***a***) in total scale (log ones); ***b***) in linear approximation the low electric field corresponds to LGD equation (10).

For the case of 1 PVDF chain, rotated and switching in the applied electric field, the reverse squared time τ^{-2} obtained, described by equation (1), depends on the electric field as a linear function at the low limit of the applied electric field values. It is shown in Fig. 8, where all the data are presented in the logarithmic scale. It could be seen that at the higher limit of the applied electric field values the behavior of the magnitude of τ^{-2} changes and its character proceeds by KAI mechanism.

For 1 PVDF chain their width is approximately equal to the value of $d \sim 0.5$ nm.

If we consider 2 PVDF chains [20, 21] – the total width is ~ 1 nm, and in this case the switching phenomena are shown in Fig. 9:

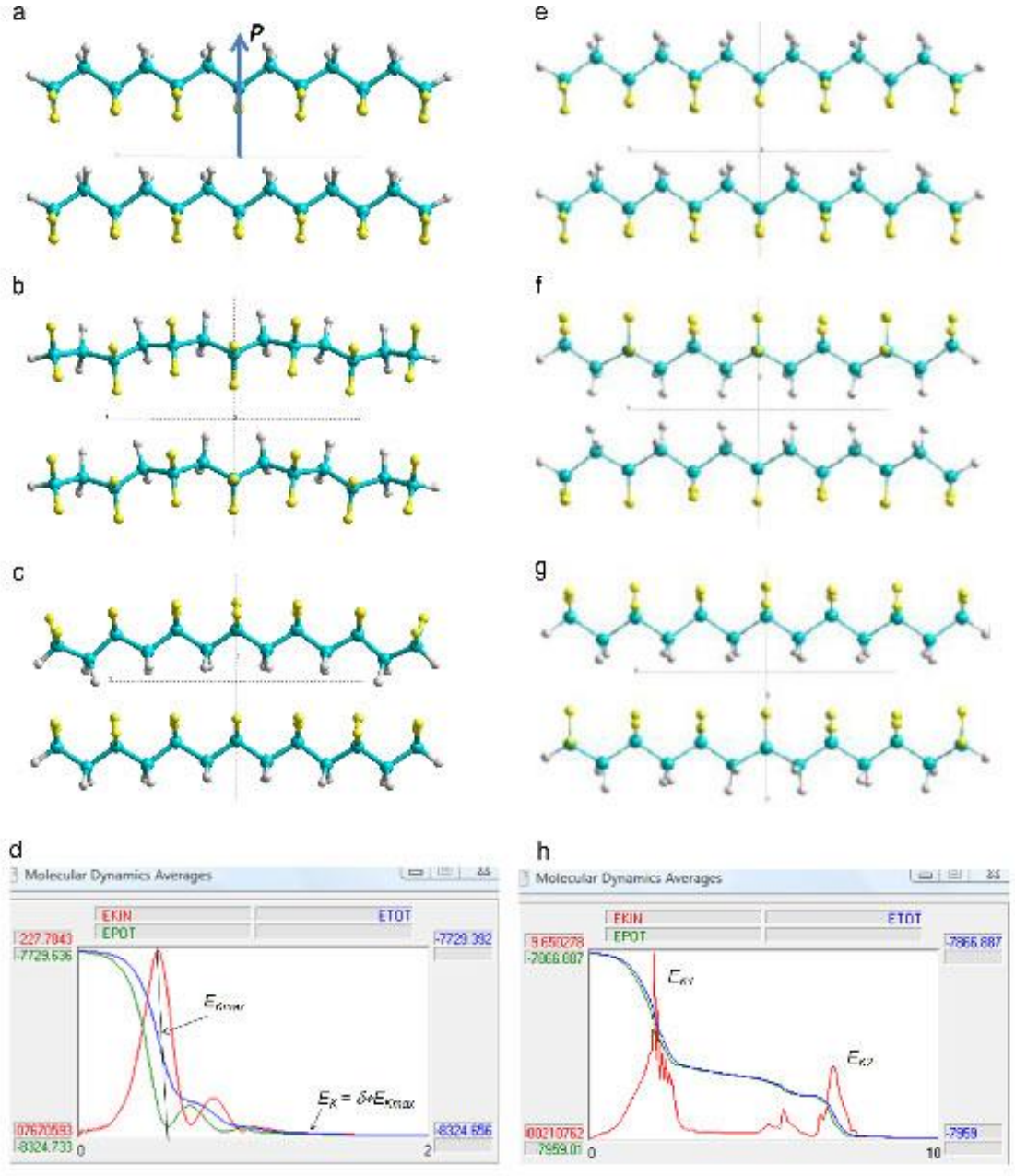

Fig. 9. Molecular model of two PVDF chains and sequence of its rotation steps under applied electric field, calculated by PM3 UHF MD run: (a)–(c) chains rotation in high electric field $E_z \sim 0.04$ a.u. ~ 20 GV/m; (e)–(g) chains rotation in low electric field $E_z \sim 0.0065$ a.u. ~ 3 GV/m, (1 a.u. ~ 500 GV/m); (d) and (h) present corresponding data of MD averaged energies during MD simulation run for both types of PVDF chains rotation.

As a result, the rotation switching time in squared reversal form τ^{-2} in logarithmic scale is shown in Fig. 10. In this case the difference between the behavior of the τ^{-2} at low and high values limits of the applied electric field *E is more clear*. Magnitude τ^{-2} has linear behavior in usual linear scale for low values of the electric field, and changes it to linear behavior in the logarithmic scale at high values of the electric field. The letter behavior corresponds to the exponential low of the dependence of the switching time from electric field in accordance with KAI mechanism and was analyzed in various papers earlier [4, 5, 20].

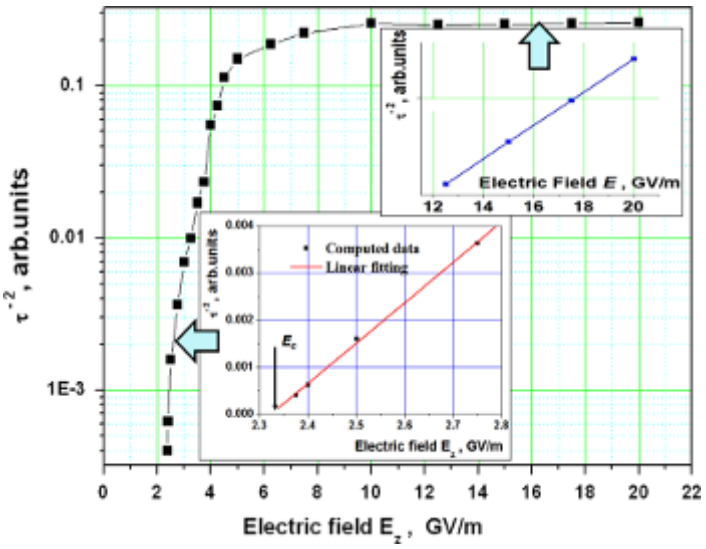

Fig. 10. Dependence of τ^{-2} on the external electric field E (τ is switching time, is presented in natural logarithmic scale along OY axis). Inserts: (down) shows the behavior of τ^{-2} in the vicinity of critical field $E = E_C \sim 2.3$ GV/m; squares are computational data, solid line coincides with Eq. (1); (above) shows the behavior of $\ln(\tau^{-2})$ at high value of external electric field E, corresponding to exponential decay with Eq. (16).

Therefore the description of the behavior of switching time at the high electric field limit demonstrates exponential decay with rise of electric field value, corresponding to known field dependence of the switching time [4, 5, 20]:

$$\tau = \tau_0 \exp\left\{-\gamma \frac{E}{E_C}\right\}, \tag{16}$$

which could be rewritten in another linear form

$$\ln(\tau^{-2}) = -2\ln(\tau_0) + 2\gamma \frac{E}{E_C} \tag{16a}$$

The most interesting result is that in the last case of 2 chains the values of the coercive electric field $E_C \sim 2.3$ GV/m > 0.5 GV/m for 1 PVDF chain.

Further computational study shows that for 4 PVDF chains it is approximately close to the same value $E_C \sim 2.3\ldots2.5$ GV/m. This effect could be explained by the interactions of dipole chains, which reduce the rotation time and increase the critical electric field which is necessary for rotation of interacting dipole chains. While for 1 PVDF chain a similar rotation in the electric field is free, without any "friction". Such effect could be called an electrostatic "dielectric friction" between interacting molecular dipoles. For the case of the 4 PVDF chains the total width is approximately d ~ 1.8 … 2.0 nm. Size dependence in this case is shown in Fig. 11.

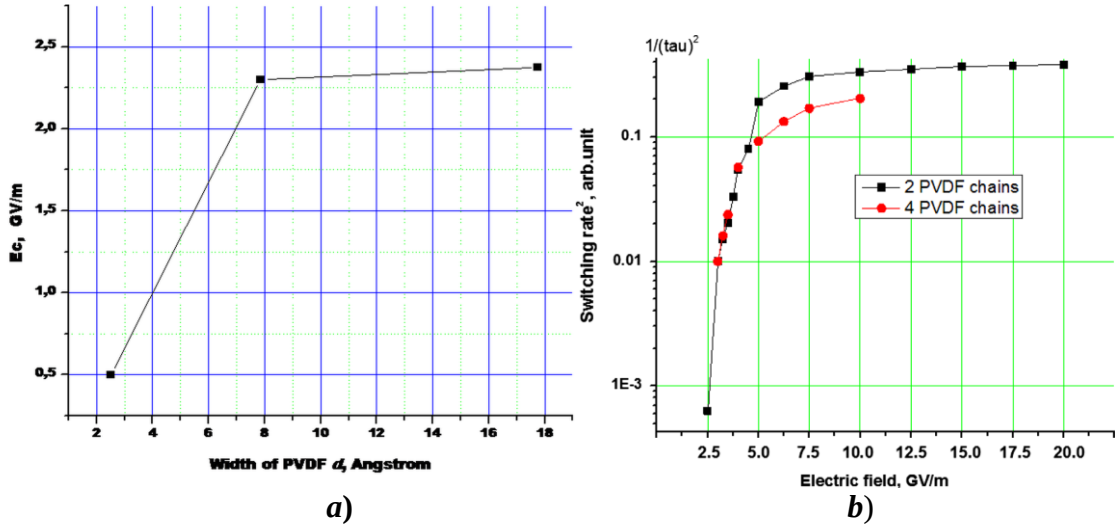

Fig. 11. Size dependence of critical field E_C from depth d for modeling (***a***) and behavior of the reversal squared time τ^{-2} from the applied electric field for both cases of the 2 PVDF and 4 PVDF chains (b).

5. DISCUSSIONS

The computational and experimental data obtained and the analysis of the polarization switching mechanisms in thin and thick polymer ferroelectric films made clearly show that there exist two main regions of the width (or depth) of the ferroelectric films:

1) ultrathin region with intrinsic homogeneous switching behavior in accordance with LGD theory;

2) a thicker region with extrinsic domain mechanism behavior of switching time corresponding to the KAI mechanism theory.

The question is only to determine most exactly the transition region sizes between these two different behavior mechanisms of switching time. Now we suppose that it is close to the value of the order of 10 nm.

But we must understand further difficulties in the investigations of these phenomena:

1) Only small sizes of width (depth) are used in these modeling and calculations. It is necessary to perform the MD run for a greater number of chains (for example, for 10 nm approximately 20 chains are required). But it is a very critical situation for computational studies, because it needs very large memory resources from the computer. Nevertheless we will try to do it in our further study. But further calculations with larger models require more time and resources.

2) If we try to compare the quantitative values of E_C for these MD simulations and for experimental data from paper [11], we can see that these values differ by approximately 10 times: E_C ~2.3 GV/m from the computational case, and only E_C ~ 0.23 GV/m for the experimental data from [11] (Fig. 12).

A question arises – why is the difference so large? Below we try to analyze and discuss this point.

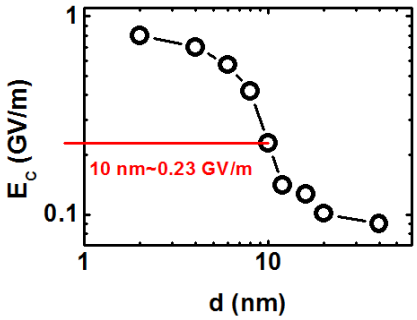

Fig. 12. Experimental data for capacitor case measurements (from [11]).

Let us analyze the situation with the experimental data obtained in [11]. They could be explained by the fact, that when modeling, we can apply not the voltage *V* (or *U* as was marked above for the case of the AFM/PFM tip), but the external electric field *E*, which in the case of the capacitor is equal to (see above in equation 15*a*):

$$E = E_0 = \varepsilon_2 \frac{V}{d_2} = \varepsilon_2 E_2 ,$$

and, therefore, in this case for $\varepsilon_2 = 10$ (in the PVDF film), the value of the outside the capacitor in the region of the applied external field (as is modeled in our case in HyperChem option for simulation of the electric field in the workspace of our molecular models) should be multiplied by ε_2 and is equal to

$$E_{0C} \sim \varepsilon_2 E_{C2} = 10\, E_{C2} \sim 10 \frac{2.3\,\text{V}}{10\,\text{nm}} \quad (\text{for } E_{C2} \sim 0.23\,\text{GV/m}).$$

Therefore, it is equivalent to the experimentally observed value of the E_{C2} ~ 0.23 GV/m at the distance (depth) of 10 nm with voltage 2.3 V on the electrodes. So, the contradiction is disappearing now and we finally have a correct result.

As a result, therefore, the best comparison presented in Fig. 5,*b* is reached for the values, which are close to $\varepsilon_1 = 5, \varepsilon_2 = 10$, $U \sim 3$ V, and all these data are close to the experimental data from [11] and are shown in Fig. 12.

Additionally, we can conclude that the data obtained are the truest results, and these data correspond to the results presented in papers [4, 5, 8, 11] as well.

6. CONCLUSION

The computational and experimental data obtained and the analysis of the polarization switching mechanisms in thin and thick polymer ferroelectric films made allow us to conclude that there exist two main regions of the width (or depth) of the ferroelectric films:

1) an ultrathin region with intrinsic homogeneous switching behavior in accordance with LGD theory;

2) a thicker region with extrinsic domain mechanism behavior of switching time corresponding to the KAI mechanism theory;

3) the value of the critical size between these two regions of the width (depth) of the ferroelectric films is approximately of the order of 10 nm.

The MD data obtained are not sufficient for exclusive final conclusion, of course. The studies should be continued further. All the results obtained are only preliminary data with first approximation values. But, this very important first step shows us a correct way for our further study and gives us data and values of the first approximation attempts.

Authors are very grateful to Fridkin V.M. for fruitful discussions of the size problems at the nanoscale level in PVDF samples.

These studies were supported by grants from the RFBR (Russia) numbers 14-31-50605 and 15-01-04924. The China part was grateful for their support from NSFC (China) project, with the Title: “The study on the new type infrared detector based on ferroelectric tunnel junction”.

REFERENCES

1. Blinov L., Fridkin V., Palto S., Bune A., Dowben P., Ducharme S. *Physics-Uspekhi*. 2000. V. 43. № 3. P. 243–258. doi: 10.1070/PU2000v043n03ABEH000639.
2. Bune A.V., Fridkin V.M., Ducharme S., Blinov L.M., Palto S.P., Sorokin A.V., Yudin S.G., Zlatkin A. Two-dimensional ferroelectric films. *Nature*. 1998. V. 391. doi: 10.1038/36069.

3. Qu H., Yao W., Zhang J., Dusharme S., Dowben P.A., Sorokin A.V., Fridkin V.M. *Appl. Phys. Lett.* 2003. V. 82. P. 4322-4324. doi: 10.1063/1.1582366.
4. Kliem H., Tardos-Morgane R. *J. Phys. D: Appl. Phys*. 2005. V. 38. P. 1860-1868. doi: 10.1088/0022-3727/38/12/002.
5. Fridkin V., Ducharme S. *Ferroelectricity at the Nanoscale. Basics and Applications*. Berlin: Springer-Verlag, 2014. 320 p.
6. Tolstousov A., Gaynutdinov R., Tadros-Morgane R., Judin S., Tolstikhina A., Kliem H., Ducharme S., Fridkin V. *Ferroelectrics.* 2007. V. 354. P. 99-105. doi: 10.1080/00150190701454669.
7. Rodrigeuz B.J., Jesse S., Kalinin S., Kim J., Ducharme S., Fridkin V.M. Nanoscale polarization manipulation and imaging of ferroelectric Langmuir-Blodgett polymer films *Appl. Phys. Lett.* 2007. V. 90. Article No. 122904. doi: 10.1063/1.2715102.
8. Bystrov V.S., Bdikin I.K., Kiselev D.A., Yudin S.G., Fridkin V.M., Kholkin A.L. *J. Phys. D: Appl. Phys.* 2007. V. 40. P. 4571–4577. doi: 10.1088/0022-3727/40/15/030.
9. Gaynutdinov R.V., Mitko S., Yudin S.G., Fridkin V.M., Ducharme S. Polarization switching at the nanoscale in ferroelectric copolymer thin films. *Appl. Phys. Lett.* 2011. V. 99. P. 142904. doi: 10.1063/1.3646906.
10. Gaynutdinov R., Yudin S., Ducharme S., Fridkin V. *J. Phys.: Condens. Matter.* 2012. V. 24. Article No. 015902. doi: 10.1088/0953-8984/24/1/015902.
11. Wang J.L., Liu B.L., Zhao X.L., Tian B.B., Zou Y.H., Sun S., Shen H., Sun J.L., Meng X.J., Chu J.H. Transition of the polarization switching from extrinsic to intrinsic in the ultrathin polyvinylidene fluoride homopolymer films. *Appl. Phys. Lett*. 2014. V. 104. Article No. 182907. doi: 10.1063/1.4875907.
12. Nakhmanson S.M., Nardelli M.B., Bernholc J. *Phys. Rev. Lett.* 2004. V. 92. Article No. 115504. doi: 10.1103/PhysRevLett.92.115504.
13. Nakhmanson S.M., Nardelli M.B., Bernholc J. *Phys. Rev. B.* 2005. V. 72. Article No. 115210. doi: 10.1103/PhysRevB.72.115210.
14. Su H., Strachan A., Goddard W.A. III. *Phys. Rev. B*. 2004. V. 70. Article No. 064101. doi: 10.1103/PhysRevB.70.064101.
15. Duan C.G., Mei W.M., Yin W.G., Liu J., Hardy J.R., Ducharme S., Dowben P.A. *Phys. Rev. B.* 2004. V. 69. Article No. 235106. doi: 10.1103/PhysRevB.69.235106.
16. Bystrov V.S., Bystrova N.K., Paramonova E.V., Vizdrik G., Sapronova A.V., Kuehn M., Kliem H., Kholkin A.L. *J. Phys: Condens. Matter*. 2007. V. 19. Article No. 456210. doi: 10.1088/0953-8984/19/45/456210.
17. Bystrov V., Bystrova N., Kiselev D., Paramonova E., Kuehn M., Kliem H., Kholkin A. *Integrated Ferroelectrics.* 2008. V. 99. P. 31–40. doi: 10.1080/10584580802107510.
18. Bystrov V.S., Paramonova E.V., Dekhtyar Yu., Pullar R.C., Katashev A., Polyaka N., Bystrova A.V., Sapronova A.V., Fridkin V.M., Kliem H., Kholkin A.L. *J. Appl. Phys.* 2012. V. 111. Article No. 104113. doi: 10.1063/1.4721373.
19. Bystrov V.S., Paramonova E.V., Bdikin I.K., Bystrova A.V., Pullar R.C., Kholkin A.L. *J. Mol. Mod.* 2013. V. 19. P. 3591–3602. doi: 10.1007/s00894-013-1891-z.
20. Bystrov V.S. *Physica B.* 2014. V. 432. P. 21–25. doi: 10.1016/j.physb.2013.09.016.
21. Gevorkyan V.E., Paramonova E.V., Avakyan L.A., Bystrov V.S. *Mathematical Biology and Bioinformatics.* 2015. V. 10. № 1. P. 131–153. doi: 10.17537/2015.10.131.
22. Egusa S., Wang Z., Chocat N., Ruff Z.M., Stolyarov A.M., Shemuly D., Sorin F., Rakich P.T., Joannopoulos J.D, Fink Y. *Nature Materials.* 2010. V. 9. P. 643–648. doi: 10.1038/nmat2792.
23. Hu Z., Tian M., Nysten B., Jonas A.M. *Nature Materials.* 2009. V. 8. P. 62-67.
24. Amer S., Badawy W. *Current Pharmaceutical Biotechnology.* 2005. V. 6. P. 57–64. doi: 10.2174/1389201053167220.
25. Callegari B., Belangero W.D. Analysis of the interface formed among the poli (viniilidene) fluoride (piezoelectric and nonpiezoelectric) and the bone tissue of rats.

Acta Ortop. Bras. 2004. V. 12. № 3. P. 160–166. doi: 10.1590/S1413-78522004000300005.
26. Tagantsev A.K., Cross L.E., Fousek J. *Domains in Ferroic Crystals and Thin Films*. New York: Springer, 2010.
27. Vizdrik G., Ducharme S., Fridkin V.M., Yudin S.G. *Phys. Rev. B.* 2003. V. 68. Article No. 094113. doi: 10.1103/PhysRevB.68.094113.
28. Kolmogorov A.N. *Izvestija Akad. Nauk Ser. Math.* 1937. V. 31. № 3. P. 355-359.
29. Avrami M. *J. Chem. Phys.* 1940. V. 8. doi: 10.1063/1.1750631.
30. Ishibashi Y., Takagi Y. *J. Phys. Soc. Jpn.* 1971. V. 31. № 2. P. 506–510. doi: 10.1143/JPSJ.31.506.
31. Ducharme S., Fridkin V.M., Bune A.V., Palto S.P., Blinov L.M., Petukhova N.N., Yudin S.G. *Phys. Rev. Lett.* 2000. V. 84. P. 175. doi: 10.1103/PhysRevLett.84.175.
32. Sharma P., Reece T.J., Ducharme S., Gruverman A. *Nano Lett.* 2011. V. 11. P. 1970–1975. doi: 10.1021/nl200221z.
33. Molotskii M. *Journal of Applied Physics***.** 2003. V. 93. P. 6234. doi: 10.1063/1.1567033
34. Kalinin S.V., Morozovska A.N., Chen L.Q., Rodriguez B.J. *Rep. Prog. Phys.* 2010. V. 73. Article No. 056502. doi: 10.1088/0034-4885/73/5/056502.
35. Tybell T., Paruch P., Giamarchi T., Triscone J.M. *Phys. Rev. Lett.* 2002. V. 89. № 9. Article No. 097601. doi: 10.1103/PhysRevLett.89.097601.

Received July 04, 2015.
Published September 27, 2015.